Journal of Applied Electrochemistry **29**: 1085–1094, 1999.

Kinetics and mechanism of the preparation of Raney® copper

A.J. SMITH*, T. TRAN and M.S. WAINWRIGHT
School of Chemical Engineering & Industrial Chemistry, University of New South Wales, Sydney, Australia 2052
*(*author for correspondence, e-mail: aj.smith@student.unsw.edu.au)*

Received 26 October 1998; accepted in revised form 9 February 1999

Key words: dealloying, focussed ion beam, selective dissolution, skeletal catalysts, structure

Abstract

Raney® copper is an active hydrogenation catalyst formed by the selective dissolution of aluminium from a Cu–Al alloy. The structure of Raney® copper is presented in a series of images taken using a focussed ion beam miller (FIB). The images show a structure consisting of a uniform three-dimensional network of fine copper ligaments. A rotating disc electrode, used to control the diffusion layer, enabled a study of the kinetics of the leaching reaction at 269–303 K in 2–8 M NaOH. Under these conditions, the reaction rate was constant and independent of hydroxide concentration. The activation energy for leaching was determined as 69 ± 7 kJ mol^{-1}. The mixed corrosion potential of the dissolving alloy has been related to the exposed copper surface area, which in turn is dependent on the leaching rate and the mechanism of rearrangement. The overall mechanism of formation/rearrangement of the Raney® copper structure was found to be mainly dissolution/redeposition of copper atoms, with surface or volume diffusion, or possibly both, playing a minor role.

List of symbols

A	is the surface area (m^2)
A_{disc}	is the flat geometric surface area of the rotating alloy disc (m^2)
A_0	is the initially formed surface area, before rearrangement (m^2)
A_{Cu}	is the exposed surface area of pure copper residue (m^2)
A_{CuAl_2}	is the exposed surface area of $CuAl_2$ alloy (m^2)
$\alpha_{H_2,Cu}$	is the transfer coefficient for H_2 evolution on Cu
$\alpha_{H_2,CuAl_2}$	is the transfer coefficient for H_2 evolution on $CuAl_2$
E	is the actual potential (V)
$E^{0'}_{H_2}$	is the formal potential for the hydrogen evolution reaction (V)
F	is the Faraday constant (96 486 C mol^{-1})
γ	is the surface free energy (J m^{-2})
i_{Al}	is the net current from aluminium (A)
i_{H_2}	is the net current from hydrogen (A)
$i_{H_2(Cu)}$	is the hydrogen current occurring on pure copper (A)
$i_{H_2(CuAl_2)}$	is the hydrogen current occurring on $CuAl_2$ (A)
$k^0_{H_2,Cu}$	is the standard rate constant for hydrogen evolution on pure copper
$k^0_{H_2,CuAl_2}$	is the standard rate constant for hydrogen evolution on $CuAl_2$
K, k_d, k_r	are proportionality constants
κ	is the 'curvature' [43, 44]
λ	is a characteristic length
n_a	is the number of electrons transferred in the rate limiting step
nq	is the charge ($2 \times 1.6 \times 10^{-19}$ C for copper ions)
R	is the gas constant (8.314 J mol^{-1} K^{-1})
r_L	is the ligament radius (m)
$r_{L,0}$	is the initial ligament radius (m)
T	is the absolute temperature (K)
t	is time (min)
V	is the volume (m^3)
x	is the rearrangement exponential
Ω	is the atomic volume

1. Introduction

Raney® catalysts, named after their inventor Murray Raney, have been well known [1–4] for most of this century. They are formed by the selective dissolution (usually by alkali) of an active metal (usually aluminium) from an alloy, leaving a noble metal residue which is an active hydrogenation catalyst [5–7]. Although Raney® nickel is by far the most popular catalytic material of this nature, Raney® copper is gaining

Raney® is a registered trademark of W.R. Grace & Co.

support, especially for the production of methanol from synthesis gas [8–13].

The preparation conditions affect the structure and composition of the catalyst, and hence its activity [7, 9, 12]. An understanding of the formation mechanism is thus highly desirable in order to obtain an optimised catalyst, or for predicting new materials that would make a better catalyst.

In the case of Raney® copper, the precursor alloy is $CuAl_2$, made by quenching a melt of 50% copper–aluminium. The aluminium is dissolved from the alloy using about 6 M NaOH at 274 K. It is known [14] that during leaching almost all of the aluminium is dissolved, leaving only one-third of the original number of atoms left to form a solid structure. The exact way, and into what structure, the copper arranges itself has continued to elude researchers.

During the dissolution of $CuAl_2$, the basic microstructure is retained, as observed by optical microscope [11, 15, 16]. Szot and Young [16] reported that the leached residue consisted of long copper rods running parallel to the leach direction. These conclusions were drawn from TEM pictures, which are difficult to obtain and interpret in three dimensions for a solid that is as porous as Raney® copper.

The formation of Raney® copper falls under a group of reactions known as 'dealloying', or 'selective dissolution'. This area has been one of heated debate for several decades regarding the true mechanisms that are operating during the reaction. Kalina et al. [17, 18] reported that Raney® copper is formed by the simultaneous dissolution of both metals, followed by the reprecipitation of the more noble metal. This mechanism, for general dealloying, was once popular, but was soon regarded as unlikely [19]. Pickering and Wagner [20–22] proposed a model based on volume diffusion, while the work by Forty and his coworkers [23–26] has extended the surface diffusion model that was originally proposed by Swann [27, 28]. Zartsyn et al. [29] have studied all three types of mechanisms from a thermodynamic/electrochemical view point, and have shown that all three are feasible, and may even occur simultaneously.

It is known [30, 31] that the leached structure of Raney® copper, once formed, undergoes rearrangement, resulting in a loss of surface area. Pickering [32] found that the same losses in surface area occur for a Cu–Au system. Tomsett et al. [31] proposed that the mechanism of rearrangement involved dissolution/reprecipitation of the copper from areas of high curvature, based on the theory of Sieradzki [33].

This study was conducted: (i) to examine the internal and external structure of Raney® copper using a focussed ion beam miller; (ii) to gain an understanding of the kinetics of leaching in the absence of diffusion limitations; and (iii) to use electrochemical measurements to elucidate the mechanism of formation and rearrangement of the Raney® structure.

2. Experimental details

The precursor alloy for all experiments was supplied by Riverside Metal Industrial Pty Ltd and consisted of Al–52.17 wt % Cu. The alloy was re-cast into rods and quenched, ensuring homogeneity. The rods were machined to exactly 20.0 mm diameter, then cut using an abrasive cut-off wheel into discs about 3 mm thick. The discs were polished to 1 μm on one face using diamond grinding pads.

The structure of Raney® copper was examined using a Hitachi S4500 field emission scanning electron microscope (FESEM) and a Micrion focussed ion beam miller (FIB). The FESEM was fitted with an energy dispersive X-ray spectroscope (EDS) for qualitative chemical analysis. Alloy discs were leached with 6 M NaOH at 274 K overnight. After thorough washing in distilled water then alcohol, the samples were transferred to the microscope via vacuum.

The mechanism of copper rearrangement was studied using a rotating disc electrode (RDE). The discs were held in a perspex holder, allowing the polished faces to freely dissolve in the leaching solution while their mixed corrosion potential was monitored against a Ag/AgCl reference electrode. The rate of reaction was followed by analysing the aluminium concentration in successive samples by ICP–AES. All measurements in this work are within a 10% error, and all potentials are reported against the Ag/AgCl reference electrode.

3. Results and discussion

3.1. *Structure of Raney® Copper*

Before leaching, the precursor alloy consists of $CuAl_2$ crystals with finely dispersed Al–$CuAl_2$ eutectic (Figure 1). After leaching, the basic microstructure is retained, however almost all of the aluminium is removed, as shown by EDS analysis. There is extensive cracking on the surface from shrinkage due to loss of material (Figure 2). This last observation agrees with Heusler [34], who reported large stresses during dealloying which may result in plastic deformation, or, in the case of a brittle alloy, fracture.

The FIB was used to mill into the surface of the leached alloy to expose the underlying structure. Figure 3 shows a 10 μm square hole milled into a leached $CuAl_2$ grain. The large crack to the left of the image is a shrinkage crack, as seen in Figure 2, while the large porous region towards the top of the image is leached $CuAl_2$–Al eutectic. This leached eutectic can be seen continuing under the $CuAl_2$ grain. The side of the milled hole shows the fine structure of the leached $CuAl_2$ grain, which would act as the active catalytic surface. Figure 4 is an image from directly above the hole shown in Figure 3, showing the structure at increasing depth as viewed from top-to-bottom. The network structure is evident here, as

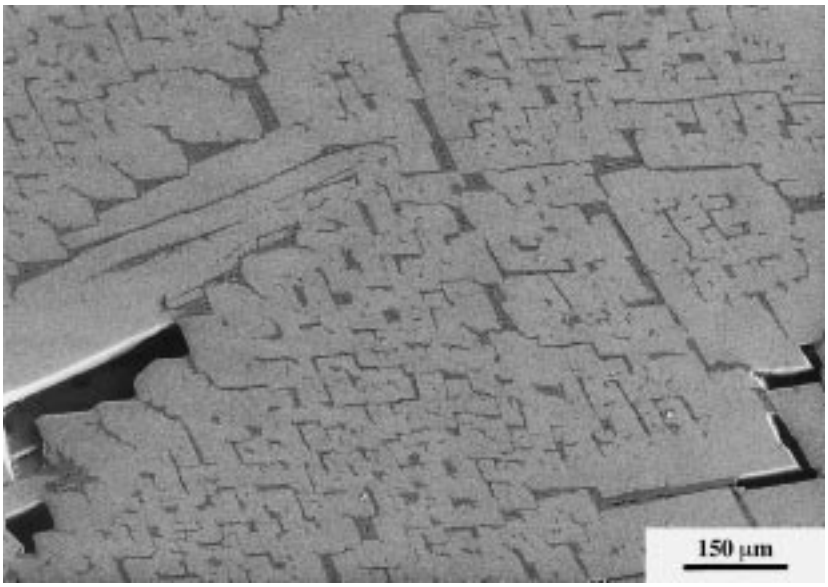

Fig. 1. FESEM micrograph showing the surface of a quenched Al–50%Cu precursor alloy. Light areas: $CuAl_2$ grains; darker areas: Al–$CuAl_2$ eutectic. Verified by EDS analysis.

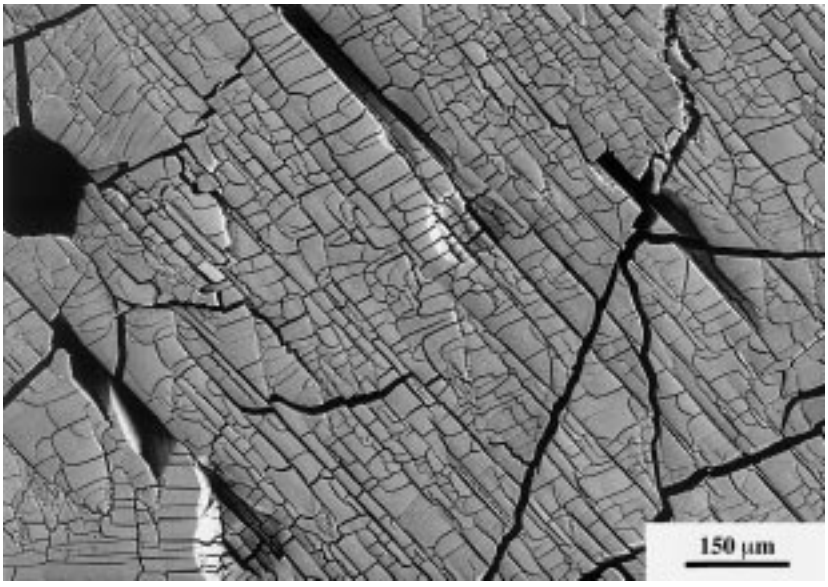

Fig. 2. FESEM micrograph showing the surface of the same alloy as in Figure 1 after overnight leaching with NaOH at 274 K. Extensive cracking is from shrinkage due to removal of aluminium. EDS analysis gives the surface composition as almost 100% copper.

is a thin surface crust. Figure 5 is a top view of a hole milled to a depth of about 1 μm. During milling, the gallium beam causes 'channelling' to occur on the sides of holes. This can be removed by applying a light 'polishing mill' to the surface at the angle of viewing. Figure 6 is a close-up of a side of a milled hole that has had a polishing mill applied to part of it. These last three images show in great detail the internal structure of Raney® copper as consisting of a fine network of three-dimensional ligaments, with a thin crust on the outside surface.

3.2. *Kinetics of dissolution*

Previous research [35] has shown that the leaching system is probably under diffusion control, which makes it hard to study the underlying mechanism. By using the rotating disc electrode, the diffusion layer is sufficiently reduced to cause the reaction to become chemically-controlled. This was verified by the independence of the reaction rate on rotation speed. In the absence of diffusion limitations, the rate of reaction was constant with respect to time (Figure 7) and independent of hydroxide concentration (Figure 8). This constant leaching rate fits reaction engineering theory [36], which predicts that the leach depth is directly proportional to time for a flat plate leaching to give a hard residue under reaction controls. Hydroxide independence rules out a rate-determining step associated with hydroxide ions. The activation energy of dissolution was found to be 69 ± 7 kJ mol^{-1} (Figure 9), confirming chemical control.

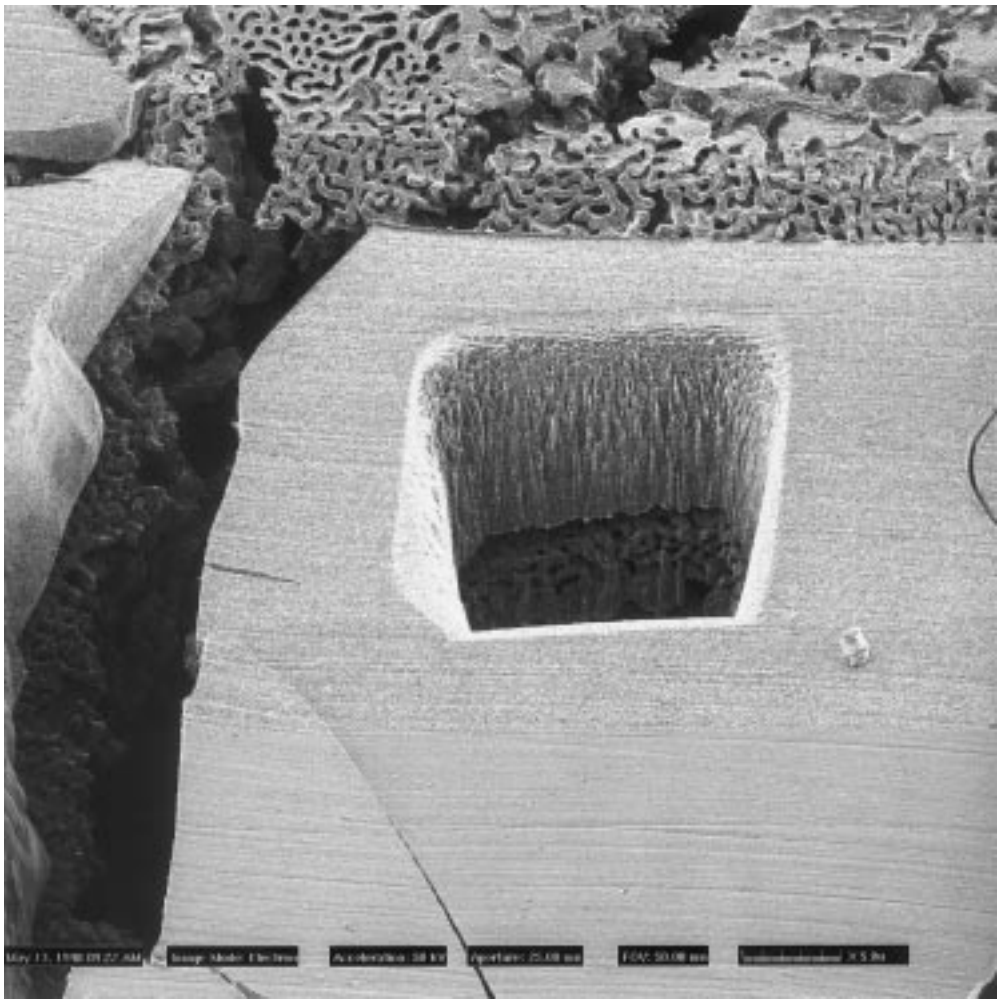

Fig. 3. FIB image of a leached alloy. Crack to left is a magnified shrinkage crack. Porous section near top of image is the leached eutectic region, and is seen continuing under the leached $CuAl_2$ grain. Fine porosity exists on the side of the 10 μm square hole milled in the centre by FIB.

3.3. *Mechanism of formation and rearrangement of structure*

The measurements of mixed corrosion potential for several experiments are shown in Figure 10. The overall half-reactions taking place are

$$CuAl_{2(s)} + 8\,OH^- \rightleftharpoons Cu_{(s)} + 2\,Al(OH)_4^- + 6\,e^- \quad (1)$$

$$2\,H_2O + 2\,e^- \rightleftharpoons H_{2(g)} + 2\,OH^- \quad (2)$$

The Butler–Volmer equation [37] gives the relation between current and potential. For the hydrogen evolution half-cell, the total current will be a combination of that occurring on the pure copper surface and that occurring on the dissolving alloy surface

$$i_{H_2} = i_{H_2(Cu)} + i_{H_2(CuAl_2)} \quad (3)$$

So, the Butler–Volmer equation is written as

$$\begin{aligned} i_{H_2} = {} & 2FA_{Cu}k^0_{H_2,Cu}\{\exp[-\alpha_{H_2,Cu}n_aX] \\ & - \exp[(1-\alpha_{H_2,Cu})n_aX]\} + 2FA_{CuAl_2}k^0_{H_2,CuAl_2} \\ & \times\{\exp[-\alpha_{H_2,CuAl_2}n_aX] - \exp[(1-\alpha_{H_2,CuAl_2})n_aX]\} \end{aligned} \quad (4)$$

where $X = (F/RT)(E - E^{0'}_{H_2})$ and E is the mixed corrosion potential. Other symbols are as given at the outset. The backward reactions are insignificant at the potentials measured, and so may safely be ignored.

The current is related to the dissolution rate of aluminium by

$$-i_{Al} = 3FA_{disc}\frac{dAl^{3+}}{dt} \quad (5)$$

Hydrogen is only produced in conjunction with the dissolution of aluminium, hence the total hydrogen current will equal the total current of aluminium dissolution: $-i_{Al} = i_{H_2}$. Combining this with Equations 4 and 5 and ignoring the backward reactions, the dissolution rate of aluminium can be related to the corrosion potential:

$$\begin{aligned} 3FA_{disc}\frac{dAl^{3+}}{dt} = {} & 2FA_{Cu}k^0_{H_2,Cu}\exp[-\alpha_{H_2,Cu}n_aX] \\ & + 2FA_{CuAl_2}k^0_{H_2,CuAl_2}\exp[-\alpha_{H_2,CuAl_2}n_aX] \end{aligned} \quad (6)$$

where X is given above. The values for α_{H_2} on both pure copper and $CuAl_2$ alloy in caustic are very similar, and the values for $k^0_{H_2}$ are of the same

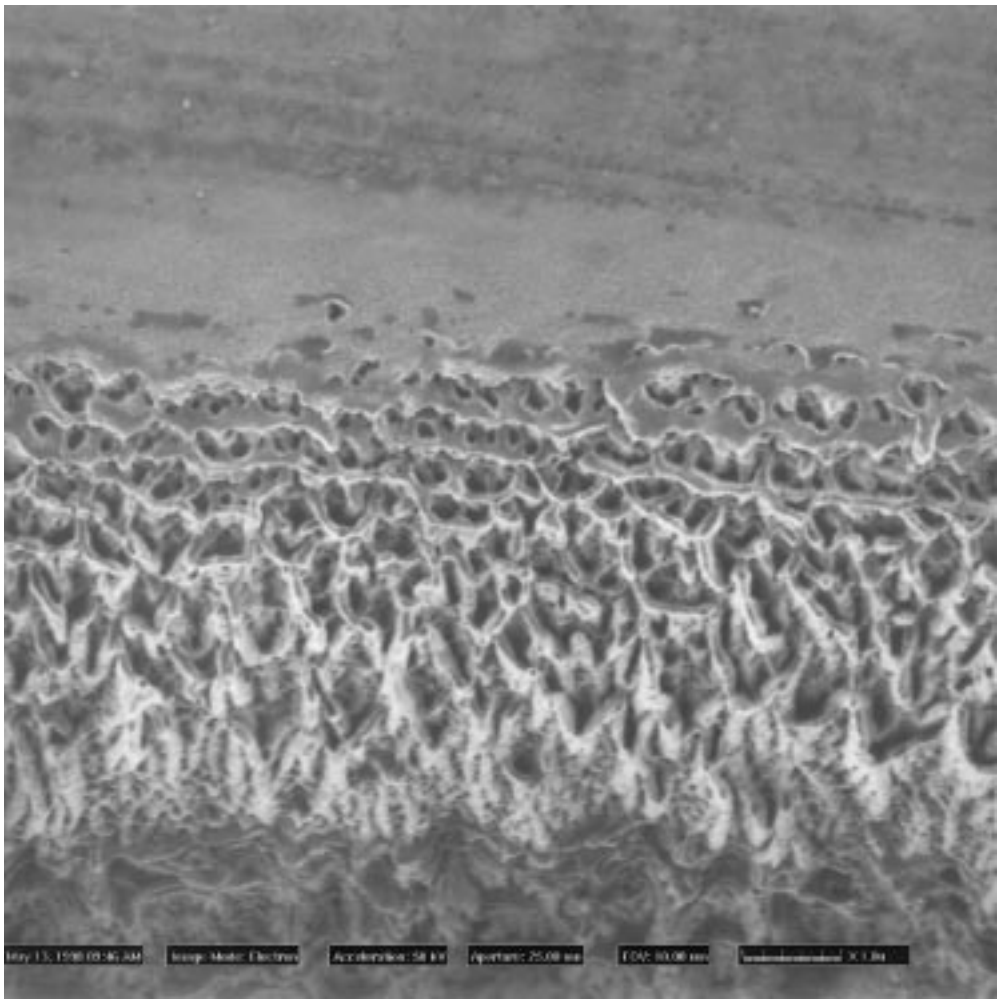

Fig. 4. Image looking down upon the top edge of the same hole as in Figure 3. Edge falls away on a curve, showing the structure of leached $CuAl_2$ with increasing depth as the image is viewed from top to bottom. A network of ligaments exists under a thin surface crust.

magnitude [38]. The respective areas of pure copper and $CuAl_2$, however, differ greatly. Ma [39] has found that the copper surface area develops extremely quickly (within a few minutes of leaching), while the unreacted alloy surface remains below the detection limits of the surface area analysis equipment. This would represent at least a 100-fold difference between the two areas, with the difference increasing with continued leaching. Thus, it appears fairly safe to assume that the total amount of hydrogen evolution occurring on the unreacted alloy surface is negligible compared to that occurring on the pure copper surface. Equation 6 now becomes:

$$3FA_{\text{disc}}\frac{\mathrm{d}Al^{3+}}{\mathrm{d}t} = 2FA_{\text{Cu}}k^{0}_{\text{H}_2,\text{Cu}}\exp\left[-\alpha_{\text{H}_2,\text{Cu}}n_{\text{a}}X\right] \tag{7}$$

substituting for X and rearranging gives

$$E = \frac{RT}{\alpha_{\text{H}_2,\text{Cu}}n_{\text{a}}F}\ln(A_{\text{Cu}}) - \frac{RT}{\alpha_{\text{H}_2,\text{Cu}}n_{\text{a}}F} \times \ln\left(\frac{3A_{\text{disc}}\frac{\mathrm{d}Al^{3+}}{\mathrm{d}t}}{2k^{0}_{\text{H}_2,\text{Cu}}}\right) + E^{0'}_{\text{H}_2} \tag{8}$$

Now, the copper surface area, A_{Cu}, varies with time. Directly after formation, it is known [30, 31] that the copper undergoes some form of rearrangement, reducing its surface area. According to Herring [40], there are four fundamental mechanisms that a material can undergo for rearrangement:

$$\text{Amorphous flow} \quad \Delta\lambda \propto t \tag{9}$$

$$\text{Evaporation and condensation} \quad \Delta\lambda \propto t^{1/2} \tag{10}$$

$$\text{Volume diffusion} \quad \Delta\lambda \propto t^{1/3} \tag{11}$$

$$\text{Surface diffusion} \quad \Delta\lambda \propto t^{1/4} \tag{12}$$

A system may involve a combination of these mechanisms, in which case the exponential will lie between the given values.

From FIB images (Figures 4–6) the final structure of the copper is a network of ligaments, cylindrical in shape. For a cylinder, with radius r_{L}, the curved surface area is related to volume by

$$A = \frac{2V}{r_{\text{L}}} \tag{13}$$

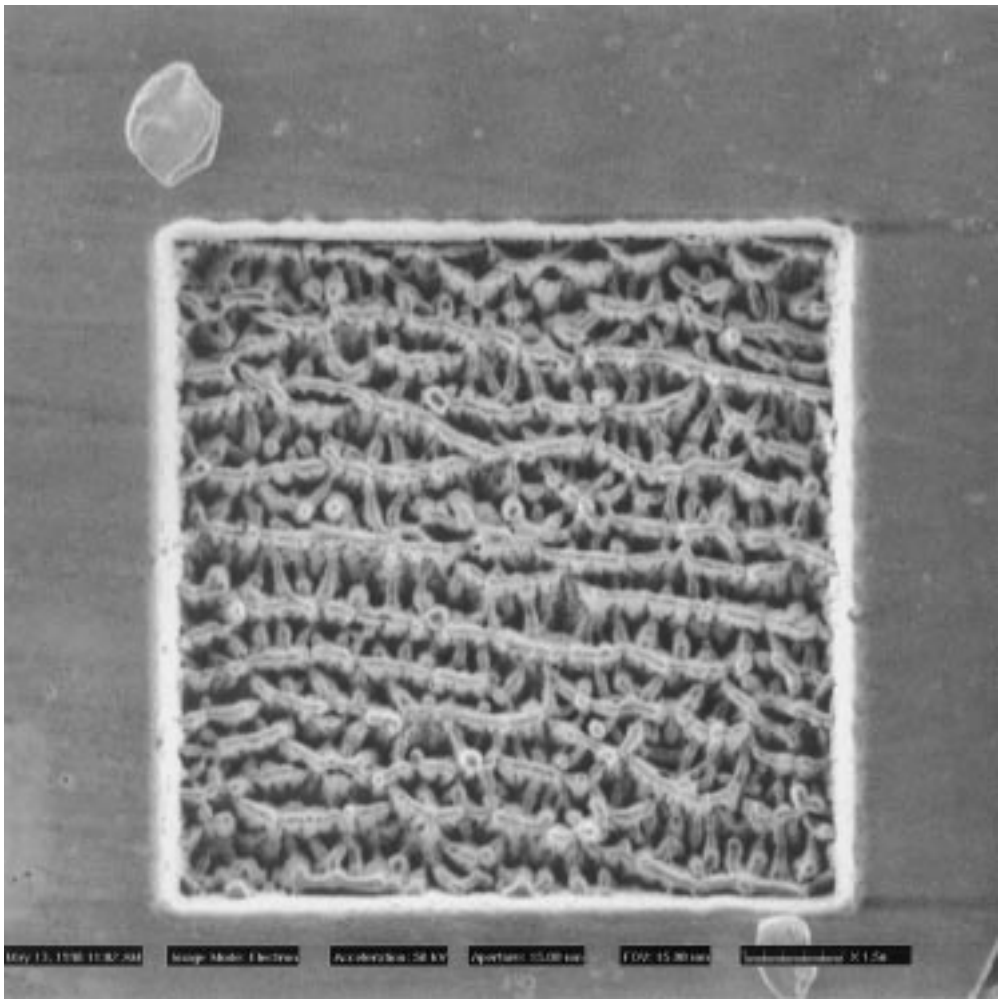

Fig. 5. FIB image of the same alloy as in Figure 3, looking directly over a new hole, about 1 μm deep.

The radius of the ligaments will increase with time according to one or more of the rearrangement mechanisms (Equations 9–12). Let the initial ligament radius be $r_{L,0}$ and the rearrangement exponential be x, giving for age t:

$$\Delta r_L \propto t^x$$

thus,

$$r_L = r_{L,0} + k_r t^x \tag{14}$$

Assuming the total volume of the ligaments will be constant (that is, no copper dissolves):

$$V = V_0 \tag{15}$$

Substituting from Equations 13 and 14,

$$A = \frac{A_0 r_{L,0}}{r_{L,0} + k_r t^x} \tag{16}$$

This gives the rate at which the copper surface area, once formed, will decrease, with x depending on the mechanism of rearrangement.

Computer simulations, similar to those presented by Sieradzki [41], verify that the surface area of the more noble metal will increase at a rate directly proportional to the dissolution rate, providing rearrangement is absent (i.e., ignoring rearrangement for now, the raw surface area exposed per unit time is directly proportional to the amount of aluminium removed per unit time). The dissolution rate is a constant (Figure 7), therefore the rate of surface area formation must also be a constant, (i.e., $A = Kk_d t$, where k_d is the dissolution rate constant, and K is a proportionality factor). Thus, if dA_0 is the amount of unrearranged surface area added during the short time interval $t_n \rightarrow t_n + dt_n$, then:

$$dA_0 = Kk_d dt_n \tag{17}$$

If the current time is t, then the age of the element is $t - t_n$. Substituting this age into Equation 16, the surface area of that element at time t will be given as

$$dA = \frac{dA_0 r_{L,0}}{r_{L,0} + k_r (t - t_n)^x} \tag{18}$$

and substituting 17,

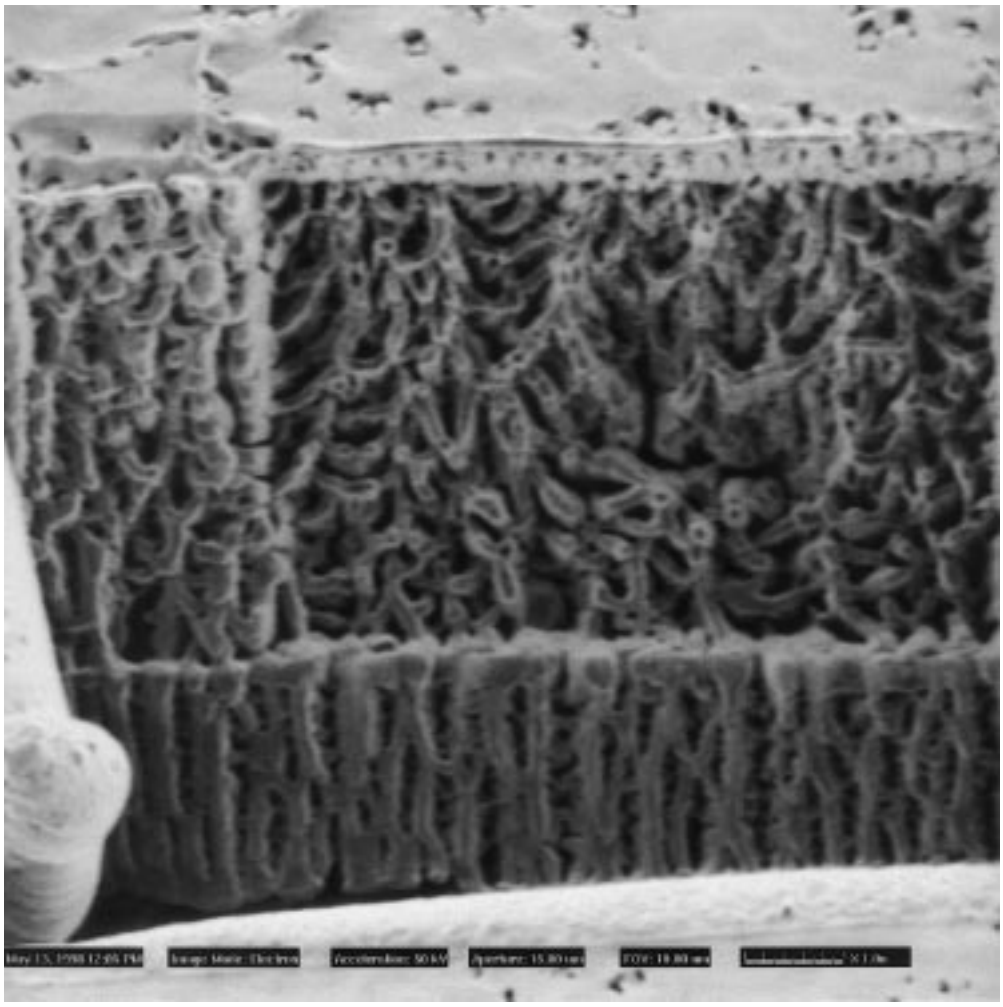

Fig. 6. FIB image of the same alloy as in Figure 3, looking directly at the side of a milled hole. A 'polishing mill' has revealed the network of copper ligaments.

$$dA = \frac{r_{L,0} K k_d dt_n}{r_{L,0} + k_r (t - t_n)^x} \tag{19}$$

The initial copper surface area is negligible [39]. Assuming the initial ligament radius is very small, then

$$r_{L,0} + k_r (t - t_n)^x \approx k_r (t - t_n)^x \tag{20}$$

so integration of Equation 19 over the range of t_n from time = 0 to current time t gives

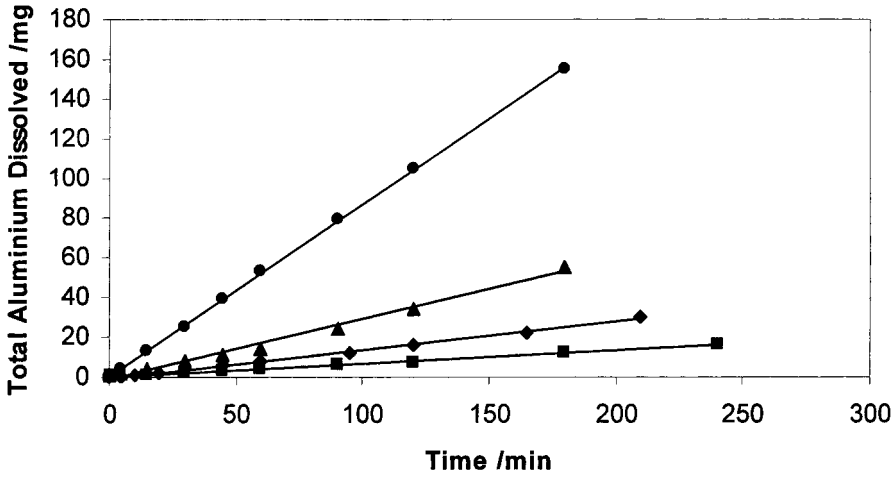

Fig. 7. Graph showing total aluminium dissolved against time. Kinetics are linear; reaction rate is given by the slope. Data obtained with 6 M NaOH at: (●) 293, (▲) 283, (◆) 274 and (■) 269 K.

$$A_{Cu} = \frac{r_{L,0} K k_d}{k_r (1-x)} t^{1-x} \quad (21)$$

Combination of Equations 8 and 21 yields the relation between corrosion potential and time. Thus,

$$E = \frac{RT(1-x)}{\alpha_{H_2,Cu} n_a F} \ln t - \frac{RT}{\alpha_{H_2,Cu} n_a F} \times \ln\left(\frac{3A_{disc} \frac{dAl^{3+}}{dt} k_r (1-x)}{2k^0_{H_2,Cu} r_{L,0} K k_d}\right) + E^{0'}_{H_2} \quad (22)$$

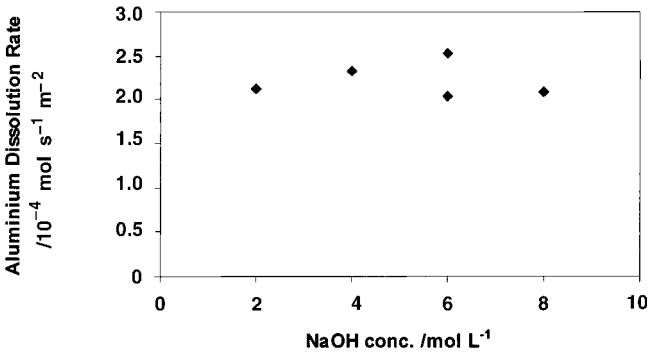

Fig. 8. Plot of reaction rate against hydroxide concentration shows independence.

Remembering that the aluminium dissolution rate is a constant, then a plot of corrosion potential, E, against the logarithm of time, $\ln(t)$, should be linear, with a slope of $RT(1-x)/\alpha_{H_2,Cu} n_a F$. The hydrogen production reaction (Equation 2) most likely follows two consecutive one-electron steps [37], and so n_a will be taken as unity. An approximate value [42] for $\alpha_{H_2,Cu}$ in 6 M NaOH is 0.37. Plots of E against $\ln(t)$ for several experiments are shown in Figure 11. From the slopes, it is possible to estimate a value for x of around 0.49 ± 0.05. This value corresponds to an 'evaporation/condensation', or more accurately, 'dissolution/redeposition', mechanism (Equation 10) for the formation, and subsequent rearrangement, of the skeletal copper structure. Although the mixed corrosion poten-

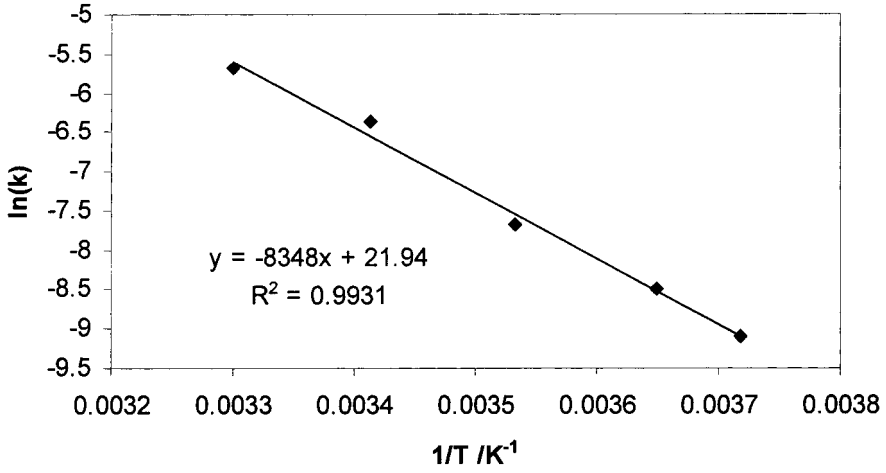

Fig. 9. Arrhenius plot for leaching reaction. Activation energy is calculated from slope as 69 kJ mol^{-1}.

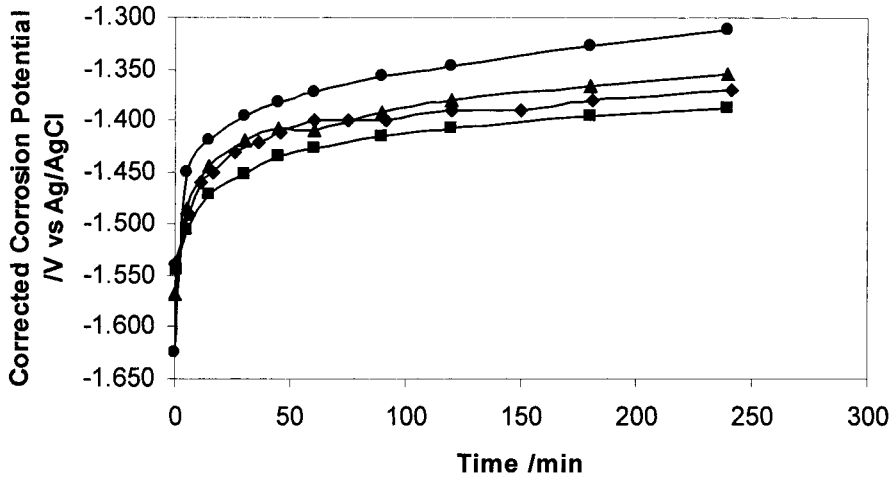

Fig. 10. Measurement of mixed corrosion potential with time. Data obtained with 6 M NaOH at: (●) 293, (▲) 283, (◆) 274 and (■) 269 K.

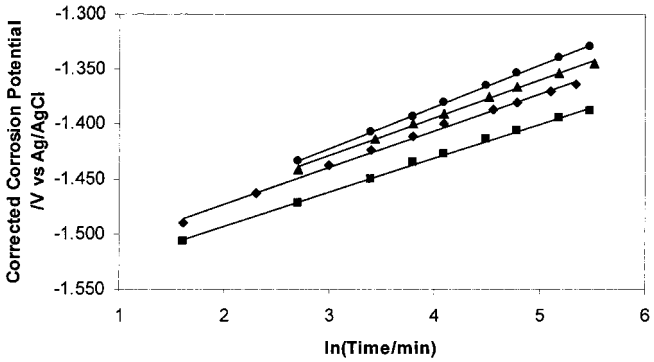

Fig. 11. Plot of potential against ln (time) for several data sets. Linearity verifies Equation 22. Key: (●) 2 M NaOH, 274 K; (▲) 4 M NaOH, 274 K; (◆) 6 M NaOH, 274 K; (■) 6 M NaOH, 269 K.

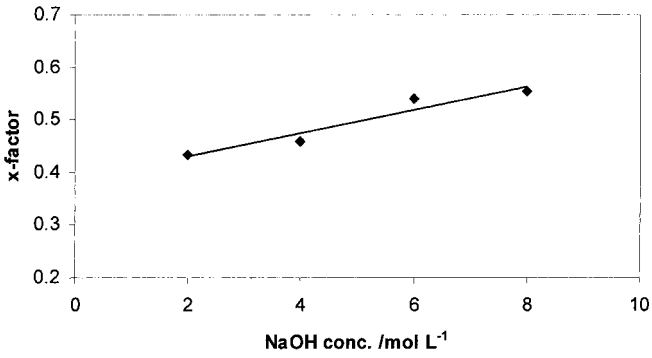

Fig. 12. Value for x is dependent on hydroxide concentration.

tial is well below the standard ionisation potential for copper, underpotential dissolution is possible through curvature effects [33].

The value for x varies with hydroxide concentration, but is independent of temperature (Figs. 12 and 13). The 'dissolution/redeposition' mechanism would depend on hydroxide for the dissolution part, however a change in hydroxide concentration should not affect the actual mechanism, only the rate at which it would occur. From the experiments, the slight change in the x-value with hydroxide concentration indicates there may be a competing mechanism. Lower hydroxide gives a lower x, so the competing mechanism is probably either surface or volume diffusion, or possibly both.

4. Conclusions

The focussed ion beam miller (FIB) has been shown to be invaluable in obtaining images of the fine structure of Raney® copper, which would otherwise be hidden under a thin surface crust, and impossible to section mechanically without possible rearrangement. The structure consists of a uniform three-dimensional network of fine copper ligaments.

The rate of leaching, in the absence of diffusion limitations, is constant with respect to time and independent of hydroxide concentration, with an activation energy of 69 ± 7 kJ mol^{-1}.

Measurement of the mixed corrosion potential has been related to the change in the exposed surface area of the copper ligaments. It was found that the overall mechanism of ligament formation/rearrangement was mainly dissolution/redeposition of the copper, with diffusion (either surface or volume, or possibly both) playing a minor role.

Acknowledgements

Financial support from the Australian Research Council is gratefully acknowledged. AJS acknowledges receipt of an Australian Postgraduate Award. The authors would like to thank A/Prof. Paul Munroe and Ms Viera Piegerova, from the Electron Microscope Unit UNSW, for their invaluable assistance in obtaining the micrographs, and Dr Liyan Ma for informative discussions. Also, thanks to Brian Cooper for the casting work and Gautam Chattopadhyay for assistance with the ICP.

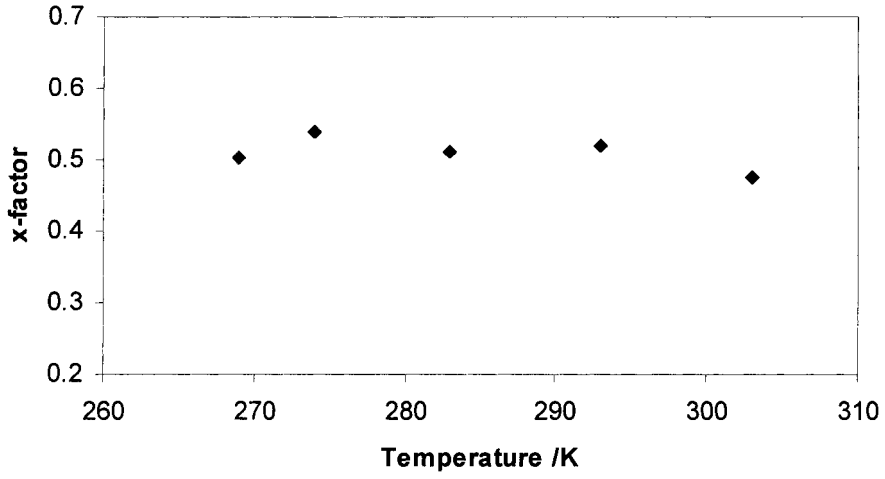

Fig. 13. Value of x is independent of temperature (i.e., mechanism of arrangement does not change with temperature).

References

1. M. Raney, *US Patent* 1 563 587 (1 Dec. 1925).
2. M. Raney, *US Patent* 1 628 190 (10 May 1927).
3. L. Faucounau, *Bull. Soc. Chim.* **4**(5) (1937) 58.
4. B.V. Aller, *J. Appl. Chem.* **7** (1957) 130.
5. M. Raney, *Ind. Eng. Chem.* **32**(9) (1940) 1199.
6. B.V. Aller, *J. Appl. Chem.* **8** (1958) 492.
7. J.A. Stanfield and P.E. Robbins, 'Raney Copper Catalysts', *in* Proc. 2nd Int. Cong. Catal., Paris (1960), 2579–99.
8. M.S. Wainwright, 'Raney Copper – A Potential Methanol Synthesis Catalyst', *in* 'Alcohol Fuels', Sydney, 9–11 Aug. (1978), p. 8–1.
9. W.L. Marsden, M.S. Wainwright and J.B. Friedrich, *Ind. Eng. Chem. Prod. Res. Dev.* **19**(4) (1980) 551.
10. J.B. Friedrich, D.J. Young and M.S. Wainwright, *J. Catal.* **80** (1983) 1.
11. J.B. Friedrich, D.J. Young and M.S. Wainwright, *J. Catal.* **80** (1983) 14.
12. H.E. Curry-Hyde, D.J. Young and M.S. Wainwright, *Appl. Catal.* **29** (1987) 31.
13. M.S. Wainwright and D.L. Trimm, *Catal. Today* **23** (1995) 29.
14. H.E. Curry-Hyde, D.J. Young and M.S. Wainwright, *J. Electrochem. Soc.* **135**(8) (1988) 1902.
15. D.J. Young, M.S. Wainwright and R.B. Anderson, *J. Catal.* **64** (1980) 116.
16. J. Szot and D.J. Young, *Philos. Mag. Lett.* **55**(3) (1987) 109.
17. M.M. Kalina, A.B. Fasman and V.N. Ermolaev, *Kinet. Katal.* **21**(3) (1980) 813.
18. M.M. Kalina, A.B. Fasman and V.N. Ermolaev, *Deposited Doc., VINITI* **1022-80** (1980).
19. M.J. Pryor and J.C. Fister, *J. Electrochem Soc.* **131**(6) (1984) 1230.
20. H.W. Pickering and C. Wagner, *J. Electrochem. Soc.* **114**(7) (1967) 698.
21. H.W. Pickering, *J. Electrochem. Soc.* **115**(2) (1968) 143.
22. H.W. Pickering, *J. Electrochem. Soc.* **117**(1) (1970) 8.
23. A.J. Forty and P. Durkin, *Philos. Mag. A* **42**(3) (1980) 295.
24. A.J. Forty, *Gold Bull.* **14**(1) (1981) 25.
25. A.J. Forty and G. Rowlands, *Philos. Mag. A* **43**(1) (1981) 171.
26. P. Durkin and A.J. Forty, *Philos. Mag. A* **45**(1) (1982) 95.
27. P.R. Swann, *Corrosion* **25**(4) (1969) 147.
28. P.R. Swann, *in* 'Localized Corrosion' (edited by B.F. Brown, J. Kruger and R.W. Staehle), NACE, Williamsburg, VA (1971), pp. 104–111.
29. I.D. Zartsyn, A.V. Vvedenskii and I.K. Marshakov, *Russ. J. Electrochem.* **30**(4) (1994) 492.
30. M. Sato and N. Ohta, *Bull. Chem. Soc. Japan* **28**(3) (1955) 182.
31. A.D. Tomsett, H.E. Curry-Hyde, M.S. Wainwright, D.J. Young, and A.J. Bridgewater, *Appl. Catal.* **33** (1987) 119.
32. H.H. Pickering, *J. Electrochem. Soc.* **115**(7) (1968) 690.
33. K. Sieradzki, *J. Electrochem. Soc.* **140**(10) (1993) 2868.
34. K.E. Heusler, *Corros. Sci.* **39**(7) (1997) 1177.
35. J.B. Friedrich, D.J. Young, and M.S. Wainwright, *J. Electrochem. Soc.* **128**(9) (1981) 1845.
36. O. Levenspiel, 'Chemical Reaction Engineering', 2nd edn (J. Wiley & Sons, Singapore, 1972), p. 372.
37. A.J. Bard and L.R. Faulkner, 'Electrochemical Methods: Fundamentals & Applications' (J. Wiley & Sons, New York, 1980), Section 3.
38. A.I. Golubev and M.N. Ronzhin, *Prot. Metals* **1** (1965) 169.
39. L. Ma, D.L. Trimm, and M.S. Wainwright, Promoted Skeletal Copper Catalysts for Methanol Synthesis *in* 'Advances of Alcohol Fuels in the World' Beijing, China 21–24 Sept. (1998), pp. 1–7.
40. C. Herring, *J. Appl. Phys.* **21** (1950) 301.
41. K. Sieradzki, R.R. Corderman, K. Shukla, and R.C. Newman, *Philos. Mag. A* **59**(4) (1989) 713.
42. M.D. Zholudev and V.V. Stender, *J. Appl. Chem. USSR* **31** (1958) 711.
43. C. Herring, Surface Tension as a Motivation for Sintering *in* 'The Physics of Powder Metallurgy' (edited by W.E. Kingston), (Bayside, L. I., New York, 24–26 Aug., 1949 McGraw-Hill Book Company).
44. W.W. Mullins, Solid surface morphologies governed by capillarity, *in 'Metal Surfaces: Structure Energetics and Kinetics', 27–28 Oct. 1962, ASM.*